

# THE INFLUENCE OF NON-ONBERBECK-BOUSSINESQ EFFECTS AND ROTATION ON TURBULENT RAYLEIGH-BÉNARD CONVECTION

**Susanne Horn**

Institute for Aerodynamics and Flow Technology  
German Aerospace Center (DLR)  
Bunsenstr a e 10, 37073 G ottingen, Germany  
Susanne.Horn@dlr.de

**Olga Shishkina**

Institute for Aerodynamics and Flow Technology  
German Aerospace Center (DLR)  
Bunsenstr a e 10, 37073 G ottingen, Germany  
Olga.Shishkina@dlr.de

**Claus Wagner**

Institute for Aerodynamics and Flow Technology  
German Aerospace Center (DLR)  
Bunsenstr a e 10, 37073 G ottingen, Germany  
Claus.Wagner@dlr.de

## ABSTRACT

The influence of rotation on turbulent Rayleigh-B enard convection in combination with non-Oberbeck-Boussinesq (NOB) effects is investigated by means of three-dimensional direct numerical simulations (DNS). For this purpose the impact of temperature dependent material properties is studied in glycerol with a Prandtl number of  $Pr = 2547.9$  within a range of Rayleigh numbers of  $10^5 \leq Ra \leq 10^8$ , and in water with  $Pr = 4.38$  at  $Ra = 10^8$ , both under no rotation and superimposed with rotation within a Rossby number range of  $0.3 \leq Ro \leq 3.0$ . The generated flow fields are analyzed with respect to deviations from the Oberbeck-Boussinesq (OB) case.

We obtain a breakdown of the top-bottom symmetry, that is, different boundary layer thicknesses, modified mean temperature profiles including an increase of the centre temperature and asymmetric velocity flow patterns for glycerol as well as for water in the non-rotating case. When the Rayleigh-B enard cell is rotated, NOB effects decrease with increasing rotation rate, but are still significant. In particular they lead to a smaller gradient of the temperature within the bulk. The Nusselt number  $Nu$  in the non-rotating NOB cases slightly decreases, while it slightly increases in the rotating ones. However, the change in  $Nu$  remains within a few percent for all cases.

## INTRODUCTION

Rayleigh-B enard convection is a common and popular example how to simplify the in general highly complex buoyancy driven flows occurring in nature as well as in engineering. That means, the fluid is considered to be confined within a rather simple geometry with a heating plate at the bottom and a cooling plate at the top and thus the flow is driven by a temperature gradient  $\Delta T$ , occasionally superimposed by rotation.

A well-established method to study this idealised problem from a mathematical and numerical point of view is to make use of the Oberbeck-Boussinesq (OB) approximation (Boussinesq, 1903; Oberbeck, 1879). This means, all material properties are assumed to be constant, in particular also the density, and correspondingly the fluid is incompressible. However, within the buoyancy term, the density varies linearly with temperature. This might indeed be admissible for certain cases, but nonetheless the range of validity of this approach is actually quite restrictive. Deviations due to the violation of the OB assumption are commonly referred to as non-Oberbeck-Boussinesq (NOB) effects.

Gray & Giorgini (1976) provided a mathematically straightforward way to calculate the validity range of the OB approximation by the requirement that certain  $\varepsilon$  factors are smaller than the requested accuracy. Since at this point we are only interested in NOB effects induced by the temperature dependencies of the material properties, these are given by

$$\varepsilon_1 = \frac{\alpha_m g H}{c_{p,m}} \frac{T_m}{\Delta T}, \quad \varepsilon_2 = \frac{\alpha_m g H}{c_{p,m}} \frac{\nu_m}{\kappa_m}, \quad (1)$$

$$\varepsilon_3 = -\frac{\Delta T}{\rho_m} \frac{\partial \rho}{\partial T} \Big|_{T_m}, \quad \varepsilon_4 = \frac{\Delta T}{c_{p,m}} \frac{\partial c_p}{\partial T} \Big|_{T_m}, \quad (2)$$

$$\varepsilon_5 = \frac{\Delta T}{\rho_m \nu_m} \frac{\partial(\rho \nu)}{\partial T} \Big|_{T_m}, \quad \varepsilon_6 = \frac{\Delta T}{\Lambda_m} \frac{\partial \Lambda}{\partial T} \Big|_{T_m}, \quad (3)$$

$$\varepsilon_7 = \frac{\Delta T}{\alpha_m} \frac{\partial \alpha}{\partial T} \Big|_{T_m}. \quad (4)$$

Here  $H$  is the height of the cylinder,  $g$  the gravitational acceleration,  $\alpha$  the isobaric expansion coefficient,  $\rho$  the density,  $\nu$  the kinematic viscosity,  $\Lambda$  the heat conductivity and  $c_p$  the specific heat at constant pressure. The indices  $t$ ,  $b$  and  $m$  here and in the following refer to the quantity at the top, the bottom and the arithmetic mean temperature  $T_m = \frac{T_t + T_b}{2}$ , respec-

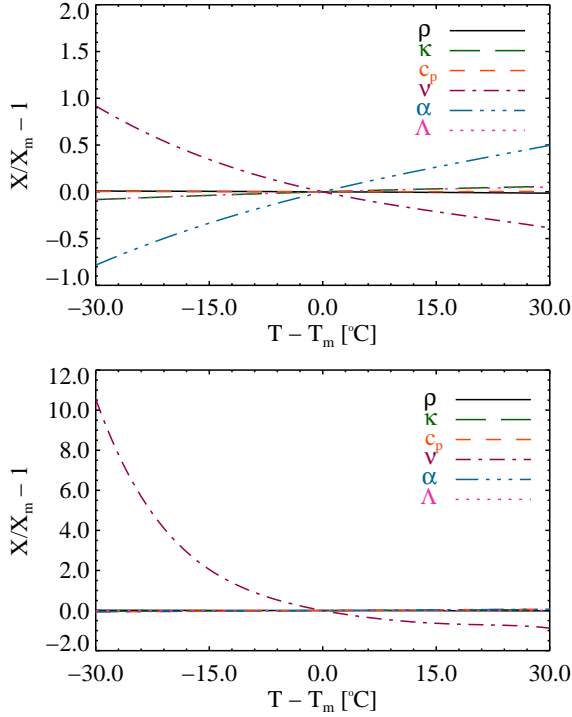


Figure 1. Relative deviations of water (upper panel) and glycerol (lower panel) properties  $X$  from their values  $X_m$  at a mean temperature of  $T_m = 40^\circ$ , according to Ahlers *et al.* (2006); black solid line, density  $\rho$ ; green dashed line, thermal diffusivity  $\kappa$ ; orange short dashed line, specific heat capacity  $c_p$ ; purple dashed dotted line, kinematic viscosity  $\nu$ ; blue dashed triple-dotted line, expansion coefficient  $\alpha$ ; pink dotted line, thermal conductivity  $\Lambda$ . Please note the very different scales, necessary for the deviations in viscosity.

tively. That means, if  $|\varepsilon_1| \dots |\varepsilon_7| \leq 0.1$ , a residual error of at most 10% is guaranteed. The factor  $\varepsilon_3$  represents the common  $\alpha\Delta T \leq 0.1$  criterion which is often quoted as sufficient criterion.

Here we focus on two different fluids, water and glycerol. The temperature dependencies of their material properties can be seen in figure 1. It is already perspicuous that here neither the isobaric expansion coefficient nor the kinematic viscosity, the thermal diffusivity and the heat conductivity can be assumed to be constant with temperature if the imposed adverse temperature difference  $\Delta T$  becomes too large. Indeed an accurate calculation yields that the factor  $\varepsilon_5$  for water and  $\varepsilon_4$  for glycerol are the demanding parameters, requiring  $\Delta T < 1$  K.

## NUMERICAL METHODOLOGY

We model turbulent Rayleigh-Bénard convection making use of a 4<sup>th</sup> order finite volume code for cylindrical domains developed by Shishkina & Wagner (2007) and performing Direct Numerical Simulations (DNS). For the purpose of investigating NOB effects, the code has been advanced by taking temperature dependent material properties into account. That is, the viscosity  $\nu$ , the thermal conductivity  $\Lambda$  and the density in the buoyancy term  $\rho$  are described by polynomials up to

cubic order in the case of water and up to quintic order in the case of glycerol,

$$\frac{X - X_m}{X_m} = \sum_i a_i (T - T_m)^i, \quad X = \nu, \Lambda, \rho \quad (8)$$

where the coefficients  $a_i$  are adopted from Ahlers *et al.* (2006), while the density  $\rho$ , except within the buoyancy term, and the isobaric specific heat capacity  $c_p$  are set constant to their values at the arithmetic mean temperature  $T_m$ . This approach is accurate for most liquids, and also for water and glycerol (see also figure 1), and accounts for the major relevant NOB effects. Hence, the flow characteristics are obtained by solving the continuity equation for incompressible fluids (5), the Navier-Stokes equations (6) and the energy equation (7) in cylindrical coordinates  $(r, \phi, z)$ , including the aforementioned material functions. Here  $\frac{D}{Dt}$  denotes the substantial derivative and the tensor  $\tilde{\tau}$  is defined via the stress tensor  $\tau$  by  $\tilde{\tau} = \frac{\tau}{\rho_m \nu}$ .

As boundary conditions for the temperature, we impose the lateral walls being adiabatic, and the top and bottom plate being isothermal, i.e. they have a constant temperature  $T_t$  and  $T_b$ , respectively. As boundary conditions for the velocity, we apply impermeability and no-slip conditions in the case of no rotation, whereas in the case of rotation the  $\phi$ -component of the velocity at the top and bottom and at the side walls is given by

$$u_\phi|_{z=H} = u_\phi|_{z=0} = \Omega r \quad \text{and} \quad u_\phi|_{r=R} = \Omega R, \quad (9)$$

with  $\Omega$  being the constant angular velocity,  $R$  the radius and  $H$  the height of the cylinder. Both times the boundary conditions are completed by setting a  $2\pi$ -periodicity in  $\phi$ -direction.

The physical parameters radius  $R$ , buoyancy velocity  $\sqrt{g\alpha_m R \Delta T}$ , temperature difference  $\Delta T$  and the matching material properties at the mean temperature, i.e.  $\nu_m, \Lambda_m, \rho_m$ , are used as reference scales for the non-dimensional equations solved numerically. Thus, the control parameters for our simulations are essentially the Rayleigh, the Prandtl and the Rossby number defined at the mean temperature  $T_m$ ,

$$Ra = \frac{\alpha_m g \Delta T H^3}{\kappa_m \nu_m}, \quad Pr = \frac{\nu_m}{\kappa_m}, \quad Ro = \frac{\sqrt{\alpha_m g \Delta T H}}{2\Omega H}. \quad (10)$$

At the moment we restrict ourselves to Rayleigh-Bénard cells with an aspect ratio of  $\Gamma = \frac{2R}{H} = 1$ .

For our performed DNS we use staggered computational meshes with nodes distributed equidistantly in  $\phi$ -direction and non-equidistantly in  $z$ - and  $r$ -direction, i.e. they are clustered in the boundary layers. We perform an *a priori* analysis of our meshes according to Shishkina *et al.* (2010). That is for water with  $Pr = 4.38$  the global mesh size is everywhere

$$h^{global} \leq \frac{H}{Ra^{1/4} (Nu - 1)^{1/4}} \quad (11)$$

and to ensure that also the NOB simulations are properly resolved twice as many nodes  $N$  as required in the OB case are

placed in the thermal and viscous boundary layer,  $\lambda_\theta$  and  $\lambda_\nu$ ,

$$N(\lambda_\theta) > 2 \cdot (0.69 Nu^{1/2}) \quad (12)$$

$$N(\lambda_\nu) > 2 \cdot (0.70 Nu^{1/2} Pr^{1/3}). \quad (13)$$

From a numerical point of view glycerol is even more challenging, since the high Prandtl number ( $Pr = 2547.9$ ) puts severe constraints on the mesh resolution. First of all the system is dominated by single plumes and second the viscous boundary layer becomes much thicker than the thermal one and eventually saturates at a certain value (Grossmann & Lohse, 2001; Breuer *et al.*, 2004; Schmalzl *et al.*, 2004). This cannot be described within theory of mesh requirements proposed by Shishkina *et al.* (2010) and furthermore it is completely unclear what happens with the boundary layer thicknesses in case of strong NOB effects. Hence, we took the criterion from Shishkina *et al.* (2010) for the mesh size in the boundary layer and used it for the whole domain and furthermore divided the mesh size by a safety factor of 2 to consider NOB effects, i.e. all cells are smaller than

$$h^{BL} = \frac{1}{2} \cdot \left[ 2^{-3/2} a^{-1} E^{-3/2} Nu^{-3/2} H \right] \quad (14)$$

$(a = 0.482, E = 0.982).$

Another issue with high Prandtl number fluids is that instabilities due to momentum diffusion are damped much faster than instabilities in the temperature and the system reacts almost instantaneously on fluctuations in the temperature resulting in a two to three orders of magnitude smaller time step than for water.

In conclusion, we note that because of the very fine meshes we were allowed to distribute our nodes equidistantly and made use of this for  $Ra = 10^7$  and  $10^8$ , which enabled us to use a bigger time step. For smaller  $Ra$  we used non-equidistant meshes where the nodes were slightly clustered in the vicinity of the walls.

## NON-OBERBECK-BOUSSINESQ EFFECTS IN GLYCEROL - WITHOUT ROTATION

The flow in large Prandtl number fluids differs to a great extent to the flow at lower Prandtl numbers at the same Rayleigh number. Instead of having a system that is dominated by a large scale circulation (LSC), the system is rather found to be in a regime dominated by plumes (Breuer *et al.*, 2004; Schmalzl *et al.*, 2004), still an LSC exists. This implies that the heat transfer is strongly convective and is consistent with the fact that inertial forces are comparatively small, while the momentum is very diffusive.

Here we want to focus on the example of glycerol, which is additionally remarkable because its viscosity is highly temperature dependent (see figure 1). For a temperature difference of  $\Delta T = 40$  K the ratio between the top and bottom viscosity at least reaches up to a factor of  $\frac{\nu_t}{\nu_b} = 16$ , whereas in water under the same condition the ratio is only about a factor of 2. However, due to the challenging computational requirements, so far DNS had been restricted to two dimensions and, interestingly, Sugiyama *et al.* (2007) found an absence of the LSC in opposite to us. In our case an, albeit weak, LSC persists, due to the three-dimensionality, indicating that 2D simulations might not entirely be adequate to capture all NOB effects.

In general one could say that NOB effects lead to the breakdown of the perfect top-bottom symmetry found in the OB case, as visualised in figure 2. Many of these asymmetries can be ascribed to the different viscosities in the cold top and hot bottom layer. That is, the lower viscosity at the warm bottom makes the plumes more prone to leave the bottom layer and they are also more mobile, i.e. faster. The cold plumes from the top show the exact opposite behaviour, i.e. they are very viscous and thus rather stuck within the cold bottom boundary layer. Furthermore the eventually emanating plumes move much slower and hence, they are much longer in contact with the ambient medium in the bulk and heat up on their way down. Ergo, the response from the system due the interplay of cold and hot plumes, is a modified mean temperature profile (see figure 3) and associated with it different boundary layer thicknesses and a deviation of the bulk temperature  $T_c$  from the arithmetic mean temperature  $T_m$ . However, the difference  $T_m - T_c$  seems to decrease with increasing  $Ra$ , although it remains significant. Another intriguing conse-

$$\frac{1}{r} \partial_r (r u_r) + \frac{1}{r} \partial_\phi u_\phi + \partial_z u_z = 0 \quad (5)$$

$$\rho_m \left( \frac{D u_r}{D t} - \frac{u_\phi^2}{r} \right) = -\partial_r p + \rho_m \left( \frac{1}{r} \partial_r (r v \tilde{\tau}_{rr}) + \frac{1}{r} \partial_\phi (v \tilde{\tau}_{r\phi}) + \partial_z (v \tilde{\tau}_{rz}) - \frac{1}{r} v \tilde{\tau}_{\phi\phi} \right)$$

$$\rho_m \left( \frac{D u_\phi}{D t} + \frac{u_r u_\phi}{r} \right) = -\frac{1}{r} \partial_\phi p + \rho_m \left( \frac{1}{r^2} \partial_r (r^2 v \tilde{\tau}_{\phi r}) + \frac{1}{r} \partial_\phi (v \tilde{\tau}_{\phi\phi}) + \partial_z (v \tilde{\tau}_{\phi z}) \right) \quad (6)$$

$$\rho_m \frac{D u_z}{D t} = -\partial_z p + \rho_m \left( \frac{1}{r} \partial_r (r v \tilde{\tau}_{zr}) + \frac{1}{r} \partial_\phi (v \tilde{\tau}_{z\phi}) + \partial_z (v \tilde{\tau}_{zz}) \right) + (\rho_m - \rho) g$$

$$\rho_m c_{p,m} \frac{D T}{D t} = \frac{1}{r} \partial_r (\Lambda r \partial_r T) + \frac{1}{r^2} \partial_\phi (\Lambda \partial_\phi T) + \partial_z (\Lambda \partial_z T) \quad (7)$$

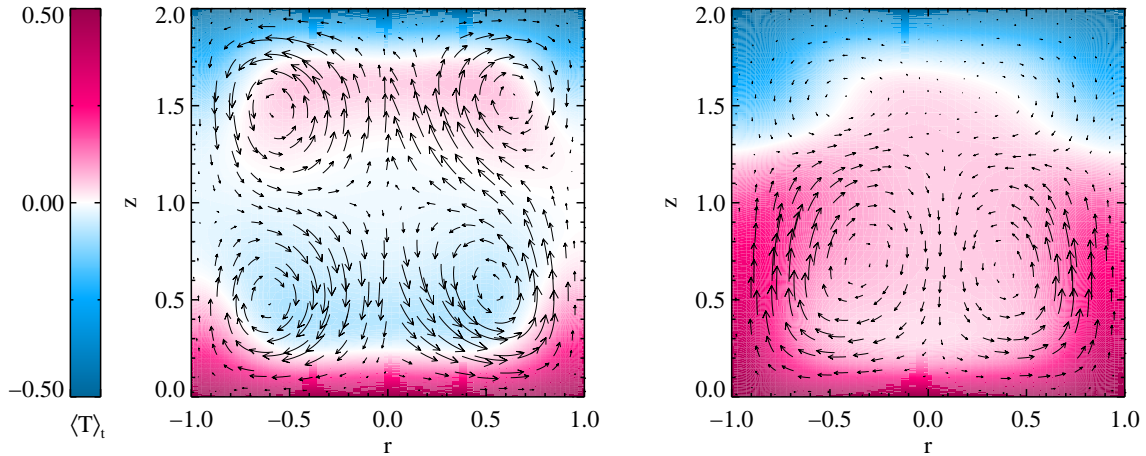


Figure 2. Slices of the temporal averaged dimensionless temperature  $T$  for glycerol with  $Pr = 2547.9$  and  $Ra = 10^5$  in the plane perpendicular to the LSC, overplotted are the velocity vectors; the left panel shows the OB case, the right one the NOB case with  $\Delta T = 40\text{K}$ , revealing the loss of symmetry when NOB effects come into play.

quence of NOB effects, nonetheless closely related to that, are the modified flow structures. Thus, in the example of  $Ra = 10^5$  we still find four convection rolls in the plane perpendicular to the LSC, but in the NOB case the upper two ones are less extended in size and have a lower velocity with their centres shifted closer to the cylinder axis. The LSC itself shows a similar deformation.

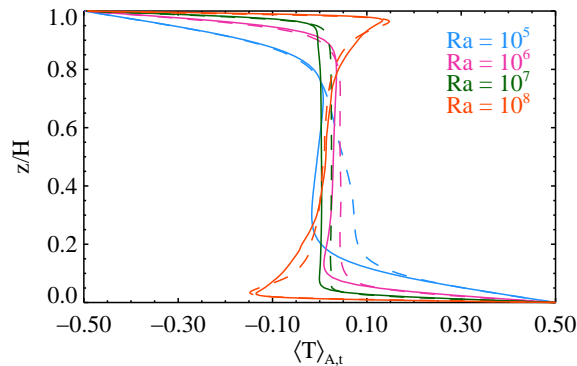


Figure 3. Mean temperature profiles, i.e. averaged in time  $t$  and in every  $r - \phi$  plane  $A$ , of glycerol for different Rayleigh numbers  $Ra$ . The solid lines indicate the OB, the dashed line the NOB cases.

### NON-OSERBECK-BOUSSINESQ EFFECTS IN WATER - WITH AND WITHOUT ROTATION

Water, while possessing rather weak temperature dependencies (see figure 1), on the other hand has the advantage of showing indeed developed turbulence at  $Ra = 10^8$  and still being sensitive to NOB effects (Ahlers *et al.*, 2006) and not to forget, it requires less computational effort. Thus, with the in-

tent to scrutinise the influence of NOB effects also on rotation, we here focus on water at a mean temperature of  $T_m = 40^\circ\text{C}$  corresponding to  $Pr = 4.38$  and four different simulation setups: without rotation ( $Ro = \infty$ ), with buoyancy dominating over rotation ( $Ro = 3.0$ ), with buoyancy and rotation equally competing ( $Ro = 1.0$ ) and eventually rotation dominating over buoyancy ( $Ro = 0.3$ ), each of them under OB and NOB conditions.

In the non-rotating case, the characteristics of the flow are similar to the above discussed case of glycerol (Horn *et al.*, 2010). Meaning, we find an enhanced centre temperature  $T_c$ , the bottom boundary layer being thinner than the top one, smaller temperature fluctuations within the bulk and a lower skewness of the temperature, as presented in figure 4. Furthermore, we also have a slightly deformed LSC and less velocity fluctuations.

But it is also known since decades (see e.g. Chandrasekhar, 1961; Julien *et al.*, 1996) that low to moderate rotation rates can stabilise the turbulent flow within a Rayleigh-Bénard cell or in other words that the turbulent fluctuations are diminished, and hence it is a fascinating question what happens if NOB and rotational effects are superimposed.

Under rotation the plumes are stretched to rather columnar vortices, also known as Ekman vortices. When  $Ro$  is decreased the amount of vortices rises, while their mean radius decreases and, depending on  $Ro$ , they are able to penetrate more or less far into the bulk. These vortices promote horizontal mixing when compared to vortical mixing, hence fully three dimensional turbulent mixing is less efficient. Thus, this increased horizontal mixing provides the reason for the persisting mean temperature gradient in the centre. To act contrary to the attenuated vertical motion caused by rotation, the upwards moving plumes also need a larger temperature difference between them and the adjacent bulk fluid, i.e. the rms temperature increases with  $Ro$ . NOB effects seem to inhibit the lateral mixing, leading to decreased rms and skewness values, as visualised in figure 4, which is consistent with the fact that the mean temperature gradient solely depends on  $Ro$  and

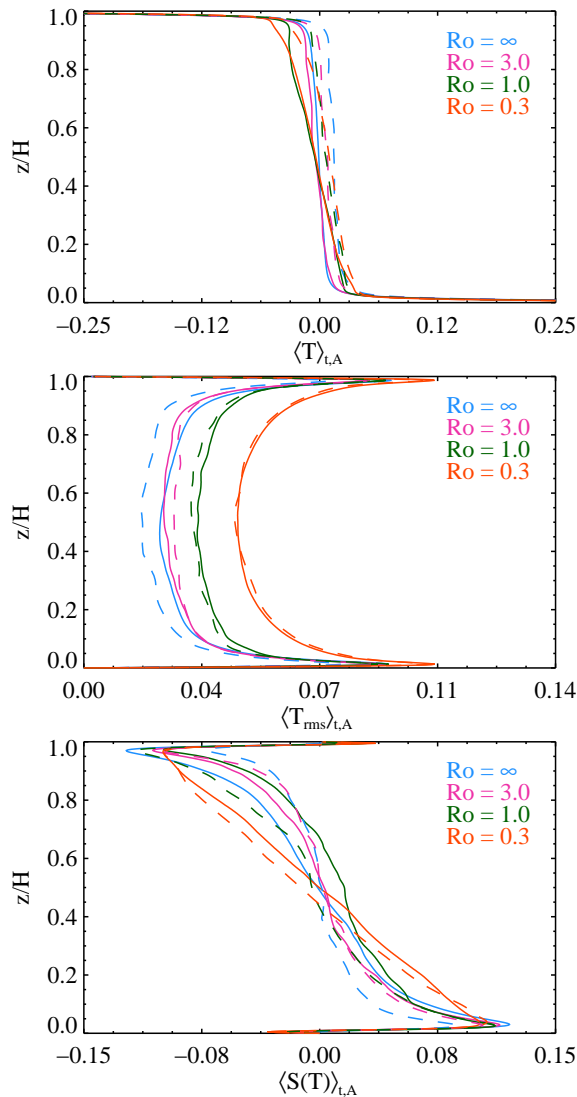


Figure 4. Mean profiles of water for different Rossby numbers  $Ro$ ,  $Ro = \infty$  corresponds to the non-rotating case. The solid lines indicate the OB, the dashed line the NOB cases. The uppermost panel shows the average temperature (note, that not the whole temperature range is shown), the middle one the temperature rms values and the lowermost one the skewness of the temperature, all averaged in time  $t$  and in every  $r - \phi$  plane  $A$  and plotted as function of the vertical coordinate.

Pr (Julien *et al.*, 1996) and these two parameters certainly vary when the material properties are not constant.

Another interesting aspect of rotating Rayleigh-Bénard convection is the enhancement of the heat flux due to Ekman pumping (see e.g. Kunnen *et al.*, 2006), the columnar vortices extract fluid from the boundary layers and thereby increase the vertical heat flux. Since they are only the prominent structures for low to moderate rotation rates, only then, of course, this enhancement can be found. Indeed, the Nusselt numbers obtained in the OB simulations, and given in table 1 with different rotation rates, show exactly this behaviour and are also

in good agreement with Zhong *et al.* (2009), albeit at another Rayleigh number. When now looking at  $Nu$  for the NOB case we obtain a similar phenomenological behaviour, but a definite increase of  $Nu$  opposing to the decrease of  $Nu$  found in the non-rotating case.

Table 1. Nusselt number,  $Ra = 10^8$ ,  $Pr = 4.38$ .

case	$Nu$
OB ( $Ro = \infty$ )	32.9
OB ( $Ro = 3.0$ )	32.8
OB ( $Ro = 1.0$ )	33.7
OB ( $Ro = 0.3$ )	37.6
NOB ( $\Delta T = 40\text{K}$ , $Ro = \infty$ )	29.7
NOB ( $\Delta T = 40\text{K}$ , $Ro = 3.0$ )	34.6
NOB ( $\Delta T = 40\text{K}$ , $Ro = 1.0$ )	35.5
NOB ( $\Delta T = 40\text{K}$ , $Ro = 0.3$ )	38.1

## SUMMARY AND CONCLUSION

In the presented study the influence of NOB and rotational effects was investigated by simulating Rayleigh-Bénard convection of water and glycerol in cylindrical cells of unity aspect ratio with different rotation rates.

Without as well as with rotation, the temperature dependency of the material properties results in asymmetric flow fields, well reflected in the increased bulk temperature, boundary layers and the convective roll structures. It is also noteworthy, that the temperature gradient maintained under rotation is diminished under NOB conditions. The deviation of the heat flux  $Nu$ , however, is within a range of a few percent, despite the fact that our simulations were performed with  $\Delta T$  severely violating the OB validity conditions. Nonetheless, it is astonishing that  $Nu$  increases when the Rayleigh-Bénard cell is rotated while it decreases if not.

**Acknowledgment** The authors acknowledge support by the *Deutsche Forschungsgemeinschaft (DFG)* under grant SH405/2-1. Furthermore, the authors would also like to thank the *Leibniz-Rechenzentrum (LRZ)* in Garching for providing computational resources on the national supercomputer HLRB-II.

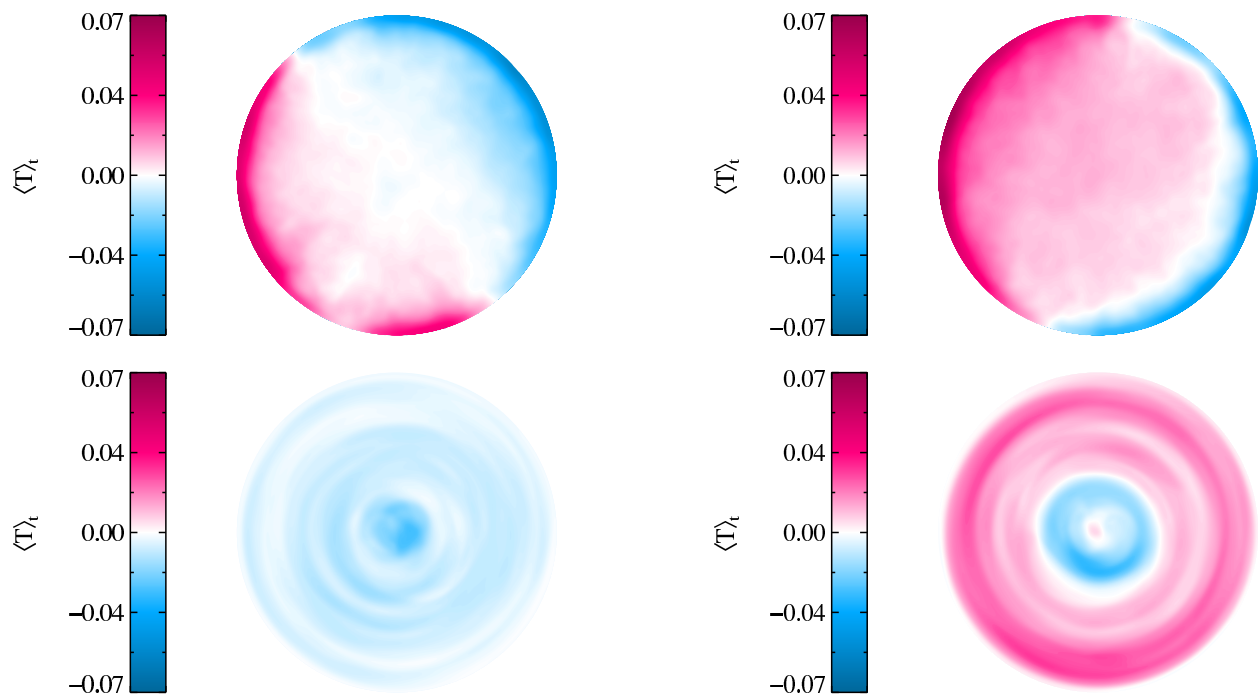


Figure 5. Cross sections of the time-averaged dimensionless temperature field  $T$  at half height of the cylinder, i.e.  $z = H/2$ , for water with  $Pr = 4.38$  and  $Ra = 10^8$ . The left panels show the OB case, the right ones the NOB case with  $\Delta T = 40$  K, the upper panels correspond to the non-rotating the lower ones to the rotating case with  $Ro = 0.3$ .

While the OB and NOB case without rotation show clear signs of a large scale circulation, the rotating cases simply show the traces of the Ekman vortices that are transported along approximately concentric trajectories. Nonetheless both NOB cases reveal an increased centre temperature  $T_c$ .

## References

- Ahlers, G., Brown, E., Fontenele Araujo, F., Funfschilling, D., Grossmann, S. & Lohse, D. 2006 Non-Oberbeck-Boussinesq effects in strongly turbulent Rayleigh-Bénard convection. *J. Fluid Mech.* **569**, 409–445.
- Boussinesq, J. 1903 *Théorie analytique de la chaleur*. Gauthier-Villars Paris.
- Breuer, M., Wessling, S., Schmalzl, J. & Hansen, U. 2004 Effect of inertia in Rayleigh-Bénard convection. *Physical Review E* **69** (2), 26302.
- Chandrasekhar, S. 1961 *Hydrodynamic and Hydromagnetic Stability*. Oxford University Press.
- Gray, D. D. & Giorgini, A. 1976 The validity of the Boussinesq approximation for liquids and gases. *Int. J. Heat Mass Transfer* **19**, 545–551.
- Grossmann, S. & Lohse, D. 2001 Thermal convection for large Prandtl numbers. *Physical Review Letters* **86** (15), 3316–3319.
- Horn, S., Shishkina, O. & Wagner, C. 2010 Non-Oberbeck-Boussinesq effects in three-dimensional Rayleigh-Bénard convection. In *Direct and Large-Eddy Simulation VIII*. In press.
- Julien, K., Legg, S., McWilliams, J. & Werne, J. 1996 Rapidly rotating turbulent Rayleigh-Bénard convection. *J. Fluid Mech.* **322**, 243–273.
- Kunnen, R. P. J., Clercx, H. J. H. & Geurts, B. J. 2006 Heat flux intensification by vortical flow localization in rotating convection. *Phys. Rev. E* **74** (5), 056306.
- Oberbeck, A. 1879 Ueber die Wärmeleitung der Flüssigkeiten bei Berücksichtigung der Strömungen infolge von Temperaturdifferenzen. *Annalen der Physik* **243** (6), 271–292.
- Schmalzl, J., Breuer, M. & Hansen, U. 2004 On the validity of two-dimensional numerical approaches to time-dependent thermal convection. *Europhys. Lett.* **67** (3), 390–396.
- Shishkina, O., Stevens, R. J. A. M., Grossmann, S. & Lohse, D. 2010 Boundary layer structure in turbulent thermal convection and its consequences for the required numerical resolution. *New J. Physics* **12**.
- Shishkina, O. & Wagner, C. 2007 A fourth order finite volume scheme for turbulent flow simulations in cylindrical domains. *Computers & Fluids* **36**, 484–497.
- Sugiyama, K., Calzavarini, E., Grossmann, S. & Lohse, D. 2007 Non-Oberbeck-Boussinesq effects in two-dimensional Rayleigh-Bénard convection in glycerol. *Europhysics Letters* **80**, 34002.
- Zhong, J.-Q., Stevens, R. J. A. M., Clercx, H. J. H., Verzicco, R., Lohse, D. & Ahlers, G. 2009 Prandtl-, Rayleigh-, and Rossby-Number dependence of heat transport in turbulent rotating Rayleigh-Bénard Convection. *Phys. Rev. Lett.* **102** (4), 044502.